

Quantifying active and resistive stresses in adherent cells

Hélène Delanoë-Ayari^{1,*} and Alice Nicolas^{2,†}

¹Université de Lyon, Université Claude Bernard Lyon 1, CNRS, Institut Lumière Matière, F-69622, VILLEURBANNE, France

²Université Grenoble Alpes, CNRS, LTM, 38000 Grenoble, France



(Received 25 March 2022; accepted 21 July 2022; published 24 August 2022)

To understand cell migration, it is crucial to gain knowledge on how cells exert and integrate forces on and from their environment. A quantity of prime interest for biophysicists interested in cell movements modeling is the intracellular stresses. Up to now, three different methods have been proposed to calculate it, they are all in the regime of the thin plate approximation. Two are based on solving the mechanical equilibrium equation inside the cell material (monolayer stress microscopy and Bayesian inference stress microscopy) and one is based on the continuity of displacement at the cell-substrate interface (intracellular stress microscopy). We show here using 3D FEM modeling that these techniques do not calculate the same quantities (as was previously assumed), the first techniques calculate the sum of the active and resistive stresses within the cell, whereas the last one only calculates the resistive component. Combining these techniques should, in principle, permit access to the active stress alone.

DOI: [10.1103/PhysRevE.106.024411](https://doi.org/10.1103/PhysRevE.106.024411)

I. INTRODUCTION

Cell motility is at the core of many physiological processes, such as embryogenesis, wound healing, etc., and pathological processes, such as metastasis in cancer [1,2]. To move, cells need to exert forces on their environment [3]. These forces originate either from cellular actomyosin contractility or from polymerization forces pushing membranes [4] (these latter forces are transmitted to the substrate on molecular clutches where actin filaments are connected to the substrates [5]). Getting information on these forces is crucial if one wants to really understand individual as well as collective cell migration. These forces are now routinely accessible using techniques such as traction force microscopy [6,7]. They are often used as a simple direct readout, marker free, of cell contractile activity. However, a closer marker of this activity should be given by the the internal mechanical active stresses generated by cells, as some of the forces exerted on the plane could theoretically be the result of friction (i.e., passive forces, resulting from cell movements) [8]. We explore in this paper the possibility of getting access to these active stresses, examining the different techniques that have been developed for measuring stresses inside the monolayer.

We make explicit the origin of the stress that each of these methods calculates, which indeed differ. We validate our approach using finite element modeling of cells submitted to active forces. We show that these different methods allow us to quantify the intracellular stress that resists cell active forces and the total intracellular stress accounting for both the active and the resistive stresses. Here we emphasize their complementarity and we make clear the limitations of these

calculations. This article is a companion paper of an experimental usage of intracellular stress calculation [9].

II. MSM, BISM, AND ISM CALCULATE DIFFERENT INTRACELLULAR STRESSES

Active forces in adherent cells generate both resistive forces inside the cells and outside, in the substrate underneath [see Figs. 1(a) and 1(b)]. Taking advantage of the well-defined mechanical properties of the substrate, and following Ref. [10], several methods have been proposed that infer intracellular mechanical stresses from the measure of the resistive force field in the substrate [11,12] or the in-plane deformation field at the surface of the substrate [13]. As we explain below, this allows quantifying the resistive stress from the cell body [13] or the total intracellular stress associated to the active and resistive intracellular forces [11,12].

The original idea of the mechanical approaches is to model cells as materials subjected to internal volume forces, the active forces mentioned above (actomyosin contractility and polymerization). When the cells are adhered to a substrate, the internal forces are transmitted to the substrate and deform it. Assuming that cell colonies as well as single cells can be modeled as a thin plate, the mechanical equilibrium writes as (Fig. 1)

$$\vec{f}_{\text{act}} + \vec{f}_c - \vec{f}_m = \vec{0}, \quad (1)$$

with \vec{f}_{act} the active cellular forces that cells build up following adhesion, \vec{f}_c and $-\vec{f}_m$, respectively, the reaction force of the cell body and the resistance of the deformable substrate opposed to these active forces, all modeled as surface forces because of the thin plate approximation. \vec{f}_m is precisely the traction stress field measured by traction force microscopy

*helene.delanoë-ayari@univ-lyon1.fr

†alice.nicolas@cea.fr

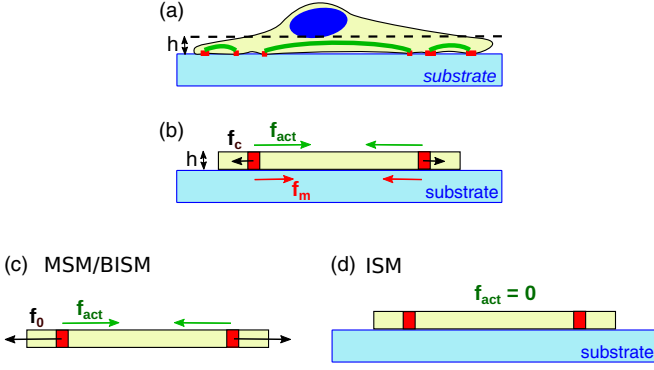


FIG. 1. (a) Schematics of a contractile cell: the cell body is submitted to internal stresses from, e.g., actomyosin filaments (in green) that are transmitted to the substrate through cell adhesions (in red). h is the thickness of the layer where the stresses transmitted to the substrate are generated. (b) Mechanical equilibrium at an adhesion point: \vec{f}_{act} is the active force generated in the cell that reaches the adhesion, \vec{f}_c is the resistance opposed by the cell material, and \vec{f}_m is the force transmitted to the substrate. (c, d) Reference states for the calculation of the intracellular stress in (c) MSM and BISM or (d) ISM. In panel (c), \vec{f}_0 is the resistance of the cell body in the absence of adhesion.

(TFM) [14]. In the present work, our aim is to characterize \vec{f}_{act} and \vec{f}_c .

Equation (1) can be reformulated in terms of the stress tensors S_{act} and S_c :

$$h \text{div} S_{\text{act}} + h \text{div} S_c - \vec{f}_m = \vec{0}, \quad (2)$$

where h is the thickness of the plate model. S_{act} is the stress tensor that is derived from the internal cellular force generation following cell adhesion. This stress can be addressed by a Gedanken experiment: Let us imagine that the cell could be detached without altering its active stress field, S_{act} . Then the cell body would contract until a size determined by the balance with the reactive stress S_0 the cell body opposes to its contraction [Fig. 1(c), with $h \text{div} S_0 = \vec{f}_0$]. Thus, $S_{\text{act}} = -S_0$ (note that S_0 is a resistive stress like S_c but that raises in the detached cells). Finally, S_c is the stress that results from the strain of the adhered cell material in response to the internal forces \vec{f}_{act} . Both S_{act} and S_c measure stresses in cells following cell adhesion. Prestresses preceding cell adhesion are not accessible here.

The original method, the monolayer stress microscopy (MSM) [10,11], addresses the resolution of Eq. (1) by building a stress tensor S_{tot} that gathers both unknown S_{act} and S_c into a single stress tensor S_{tot} :

$$S_{\text{tot}} = S_{\text{act}} + S_c, \quad (3)$$

$$h \text{div} S_{\text{tot}} = \vec{f}_m. \quad (4)$$

Equation (4) is underdetermined [15]. An additional relationship between the stress components is added by assuming that the cellular material has a linear elastic rheology [11,16]. In line with MSM, Bayesian inference stress microscopy (BISM) was proposed [12]. It also solves the equilibrium Eq. (4) but accounts for the noise in \vec{f}_m and does not assume

a rheological model a priori for the cell material. Underdetermination of Eq. (4) is resolved by using Bayesian inversion and assuming that S_{tot} has a Gaussian distribution. BISM then introduces a regularization step that allows limiting the contribution of noise in the calculated stress tensor. The rheological properties can be inferred a posteriori, by comparing the temporal derivatives of the elastic strain tensor and the spatial gradient of the velocity field in the cell material [12].

Differently, intracellular stress microscopy (ISM) addresses the quantification of the resistive component of the intracellular stress, S_c , that opposes the contraction of the adhered cell [13]. This approach calculates the increase in stress that occurs in a different Gedanken experiment, where the adherent cells go from a relaxed state ($f_{\text{act}} = 0$) to a tense state ($f_{\text{act}} \neq 0$) with constant shape [Fig. 1(d)]. When the cell is modeled as a thin elastic plate, it is straightly obtained by differentiating the displacement field of the neutral plane of the plate [17]. This approach can be extended to viscoelastic rheology when the cell material behaves like a Maxwell fluid, a rheological behavior that was for instance reported in flowing epithelial monolayers [18]. When the basal surface of the cell material is uniformly adhered to the substrate, either by integrin-mediated adhesions, non specific adhesions or other types of adhesive machinery such as lectins [9,19], the displacement field of the neutral plane of the plate is identical to the displacement field on the top of the substrate. The resistive stress then writes as

$$S_c = \begin{pmatrix} \sigma_{xx} & \sigma_{xy} \\ \sigma_{xy} & \sigma_{yy} \end{pmatrix},$$

$$\text{with} \begin{cases} \sigma_{xx} &= \frac{E_c}{1-\nu_c^2} \left(\frac{\partial u_x}{\partial x} + \nu_c \frac{\partial u_y}{\partial y} \right), \\ \sigma_{yy} &= \frac{E_c}{1-\nu_c^2} \left(\frac{\partial u_y}{\partial y} + \nu_c \frac{\partial u_x}{\partial x} \right), \\ \sigma_{xy} &= \frac{E_c}{2(1+\nu_c)} \left(\frac{\partial u_x}{\partial y} + \frac{\partial u_y}{\partial x} \right), \end{cases} \quad (5)$$

where (x, y) are the in-plane coordinates, E_c and ν_c are the Young's modulus and the Poisson's ratio of the cell material of thickness h , and $u_{x,y}$ are the in-plane components of the displacement field on top of the substrate. The displacement field is measured as in TFM, by the use of fluorescent markers embedded in the substrate. As a consequence of Eq. (5), implementation of ISM requires to know the Young's modulus of the cell E_c and its Poisson's ratio ν_c but is independent of the thickness of the contractile plate, h .

MSM or BISM and ISM thus do not address the same intracellular stresses. MSM or BISM calculates the bidimensional total stress tensor $h S_{\text{tot}} = h(S_{\text{act}} + S_c)$ [Eq. (4)], while ISM quantifies the Young's modulus-normalized resistive stress tensor S_c/E_c [Eq. (5)].

While being different quantities, both types of stresses can be evaluated on the very same experiment, and are based on very compatible assumptions; they both assume some contacts between the cell and the substrate for force transmission and for continuity of the displacement field. In MSM or BISM, forces exerted by the cells appear as boundary conditions in Eq. (4) (it is not a continuity in stress), and in ISM, the continuity in displacement is considered which is by no mean a continuity in deformation.

In the following, by using 3D FEM, we compare the two approaches for calculating intracellular stresses and

evaluate their consistency. The first approach was tested by using BISM and not MSM, as experimentally, TFM can only provide \vec{f}_m with a nonnegligible noise level of more (and often much more) than 10% [20], and BISM explicitly handles the noise level in its formulation. In any case, as both MSM and BISM are based on the same equation [Eq. (4)], they should provide similar results as already shown by Nier *et al.* [12].

III. USING 3D FEM TO COMPARE THE DIFFERENT CALCULATIONS

Since MSM, BISM, and ISM address different intracellular stresses, we built a finite elements simulation to calculate these stresses. This approach had already been attempted in Nier *et al.* [12]. In this paragraph we analyze this former simulation and show that it can only compute S_c but not S_{tot} . We then propose a different simulation that allows obtaining S_c and S_{tot} from 3D FEM.

The simulation in Ref. [12] was conceived as follows: the cell monolayer is modeled as a 2D square or disk of either a pure viscous or elastic material. Cellular contractility is modeled as external forces (random dipoles distributed inside the geometry of interest). The substrate is included in the simulation through its interaction with the cells, and enters like a friction term proportional to the velocity (viscous case) or to the displacement (elastic case, the cells are then firmly attached to the substrate composed of 1D springs). BISM and MSM stresses were calculated by solving $h\text{div}S = \vec{t}$, with $\vec{t} = -\vec{f}_{\text{act}} + \xi\vec{u}$ being the forces that act on the cells and \vec{u} the displacement field of the 2D material (note that there is a minus sign error in the equation used in the supplementary of Ref. [12]). Compared to Eq. (1), \vec{t} is therefore the resistive force that opposes the active contraction, $\vec{t} = -\vec{f}_{\text{act}} + \vec{f}_m = \vec{f}_c$, and $S = S_c$. Thus, the modeling proposed in Ref. [12] allows to calculate the reactive stress S_c by two means, either directly with differentiating the displacement field (ISM approach, denoted MSMu in Ref. [12]) or by solving $h\text{div}S_c = \vec{f}_c$. Consistently, BISM, MSM, and ISM gave very similar results. Figure S9 in Ref. [12] shows that the calculated stresses localize identically for all the methods, either in the elastic or in the viscous cases. Their amplitudes nevertheless differ but this indeed comes from different choices of the rheological parameters in between the tests: For instance, for the viscous case, first and second viscosities are taken equal in the FEM simulation ($\eta = \eta'$) leading to an equivalent Poisson's ratio of 0.25 while the equivalent Poisson's ratio is taken at 0.5 for MSM or ISM; in the same way, the Young's modulus of the cells chosen for ISM and MSM differs from those chosen for BISM (ISM: $E_c = 1$ kPa, $\nu_c = 0.5$, and h not given, but the only value available is $5 \mu\text{m}$ leading to $hE_c = 5$ kPa μm ; for MSM, $E_c = 10$ kPa, $\nu_c = 0.5$, and $h = 5 \mu\text{m}$, MSM will then compare very well with the FEM simulation in the elastic case as its result only depends on the value of ν_c , and both are taken equal; BISM, in the elastic case, $hE_c = 100$ kPa μm or $hE_c = 10$ kPa μm and $\nu_c = 0.5$). The reason for the failure of the previous simulation to address both S_c and S_{tot} and model a true experiment comes from the fact that S_{tot} is only meaningful when the cells are adhered to a substrate. Otherwise, as detailed in Sec. II, $S_{\text{tot}} = 0$ as the intracellular resistive

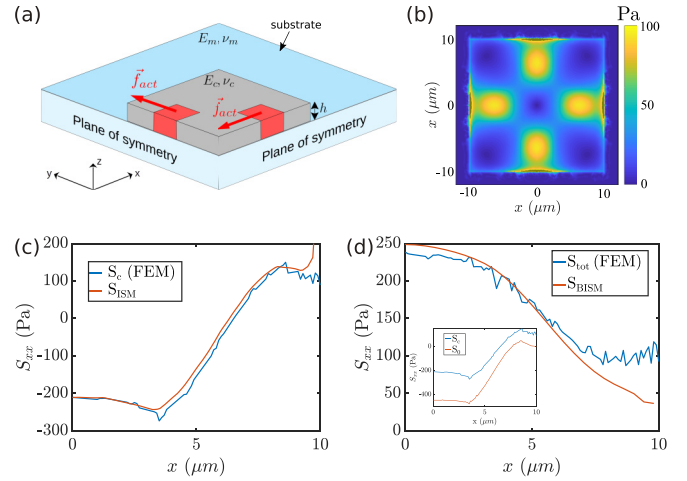


FIG. 2. FEM calculation of intracellular stresses in an elastic plate ($E_c = 5$ kPa, $\nu_c = 0.5$, $h = 1 \mu\text{m}$) bound to a deformable substrate ($E_m = 1$ kPa, $\nu_m = 0.5$). (a) Schematics of the numerical experiment. The plate is submitted to contractile and tensile force dipoles respectively along the x and y axis with truncated Gaussian profile (amplitude 1 kPa, standard deviation $2 \mu\text{m}$) concentrated in $5 \mu\text{m}$ wide squared dots. (b) Amplitude of the surface stresses \vec{f}_m on the substrate. (c) Comparison of the intracellular resistive stress S_c calculated with FEM and with ISM [S_{ISM} , Eq. (5)]. (d) Comparison of the total intracellular stress $S_{\text{tot}} = S_c - S_0$ and BISM calculation S_{BISM} [Eq. (4), regularization parameter $L = 0.003$]. The inset shows the profiles of $S_0 = -S_{\text{act}}$ and S_c used in the calculation of S_{tot} .

stress $S_c = S_0$ balances the active stress S_{act} : in the absence of anchorage to a substrate, $\vec{f}_{\text{act}} + \vec{f}_0 = \vec{0}$ [Fig. 1(c)].

To solve this issue, we thus proposed a model where the cell (or equivalently the cell colony) is modeled as thin plate uniformly bound to the substrate [Fig. 2(a)]. The dimensions of the thin plate were chosen so that the deformation field is fairly uniform in the thickness of the cellular material (square elastic sheet of size $30 \times 30 \mu\text{m}^2$ and $1 \mu\text{m}$ in thickness). We focused on the elastic case, with Young's modulus $E_c = 5$ kPa and a Poisson's ratio $\nu_c = 0.5$. The thin plate is sitting on top of an elastic gel (the substrate) which is modeled as a thick elastic parallelepiped (size $200 \times 200 \times 100 \mu\text{m}^3$ in (x, y, z) , with Young's modulus $E_m = 1$ kPa and a Poisson's ratio $\nu_m = 0.5$). A contractile dipole is positioned along the x axis, composed of Gaussian forces of amplitude 1 kPa and width σ adjusted between 0.25 and $2 \mu\text{m}$. A tensile dipole is set on the y -axis with the same amplitude and width.

IV. DETAILS ON THE ROBUSTNESS OF ISM AND BISM CALCULATIONS

A. Calculation methods

We used Comsol Multiphysics 4.2 to implement finite element modeling. The 3D FEM calculation provides the displacement field at the interface between the cell and the substrate. This displacement field was used to calculate the intracellular stresses S_c and S_{tot} using ISM and BISM as would be done with experimental data [9]. These calculations were performed with Matlab. All these codes are freely available at Ref. [21]. The sampling was chosen following

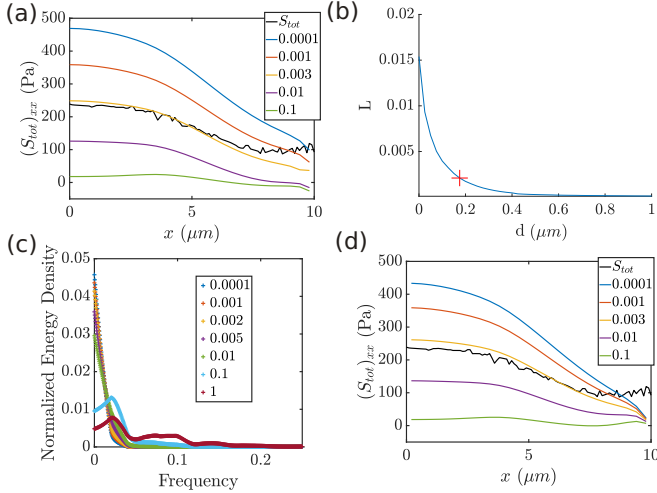


FIG. 3. Understanding BISM. (a) Calculation of S_{tot} with BISM. The FEM calculation is shown in black. The other colors refer to values of the regularization parameter L . Boundary conditions at the edges of the plate are provided by the surface forces \vec{f}_m . (b) L values calculated with Eq. (6), where the noise level outside of the cell is quantified in a mask at a distance d from the plate boundaries. The optimum for L is chosen at the maximum of curvature in the curve (red cross). (c) Increasing the regularization parameter L in BISM calculation filters the low frequencies. The colors refer to values of L . (d) Same calculation as in panel (a) but with assuming zero stress at the edges of the plate, as in Ref. [12].

Shannon criterion: the displacement field was interpolated on a sampled regular grid with a frequency more than twice the maximal frequency obtained from the FEM calculation. The resistive stress field S_c was obtained from ISM, by differentiating the in-plane displacement field retrieved from the 3D FEM calculation using a Sobel approximation of the derivative [Eq. (5)]. S_{tot} was obtained from BISM by solving Eq. (4). Traction stresses \vec{f}_m were first calculated using Fast Fourier Transform, following Butler *et al.* [22]. We took $\nu_m = 0.49$ for the calculations. The total intracellular stress S_{tot} was then calculated following Ref. [12]. As it is quite demanding on computer memory, we used a grid of 50×50 pixels to calculate the stress, which enables a rather fast computation, to perform many different tests in a reasonable amount of time. Boundary conditions were enforced in the prior to correspond to the surface forces \vec{f}_m at the edges of the cell. The hyperparameter ensuring $\sigma_{xy} = \sigma_{yx}$, was set to 10^3 as was done in Ref. [12]. The result is shown in Fig. 3(a).

B. Choosing the regularization parameter in BISM

As detailed in Ref. [23], the choice of the optimal parameter for equation form like Eq. (4) is far from obvious. It is to be noted that the L-curve criterion is not consistent with the Morozov discrepancy principle here (which states that Eq. (4) cannot be solved with a better accuracy than the noise on \vec{f}_m), as it gives a dominant weight to the accuracy of the equilibrium equation Eq. (4), omitting that the right-hand term, \vec{f}_m is a noisy, inaccurate, data. We thus chose to calculate the regularization parameter L using the χ^2 estimate [7] which considers the noise level of the right-hand term in Eq. (4). In

BISM, this criterion expresses as $L = \ell^2 s^2 / s_0^2$, with ℓ the size of the grid sampling for the calculation of S_{tot} , s the standard deviation of the noise of \vec{f}_m , and s_0 the standard deviation of the calculated stress hS_{tot} [12]. Since s_0 is unknown, an additional criterion is required. Based on Eq. (4), we estimated $s_0 \simeq \ell s_1$, with s_1 the standard deviation of \vec{f}_m . Then L is simply obtained from \vec{f}_m stress field distribution and the quantification of its noise level out of the cell boundaries:

$$L = s^2 / s_1^2. \quad (6)$$

To calculate the noise, we used the values of the surface forces \vec{f}_m outside of the cell boundaries (it should be zero if the calculation was perfect, which of course is not the case.) However, the calculation appeared trickier than for real data coming from experiments [9]. Here, the noise level sharply decreased with distance from the plate. Thus, defining the proper position of the boundary appeared mandatory to ensure that the captured noise is not the spread force signal unavoidable with finite element calculation but still is representative of FEM-induced noise. This issue is specific to FEM calculation and is not met in experimental cases where the noise around the cell is fairly uniform (see Ref. [9]). To this end, noise statistics was quantified out of the cell in regions whose distance to cell edges was varied. L values were then obtained with Eq. (6) in dependence on this distance [Fig. 3(b)]. L was considered optimal at the maximal curvature of this decreasing curve as it is the place of best compromise between attenuated force signal and maximal noise level. For the values modeled in Fig. 2(a), we obtained a regularization parameter $L = 0.002$ which consistently corresponds to the best choice for the regularization parameter compared to FEM calculation of S_{tot} [Fig. 2(d)].

C. Effect of noise in the calculation of S_{tot} and S_c

Noise strongly impacts the calculation of the force field in TFM. This problem was addressed by using regularization schemes [6,7] or a filtering in the Fourier space [22]. These regularization schemes were shown to filter high frequencies [20,24]. Noise issues keep also critical in the calculation of the intracellular stresses and we questioned how noise impacts ISM and BISM calculations. ISM is based on the derivative of the displacement field. It is therefore very sensitive to high-frequency noise. A filtering is applied by the use of the Sobel approximation in the calculation of the gradients. We showed in a companion paper [9] that experimentally, the dispersions of $\text{div}S_c$ and \vec{f}_m are similar. The fact that $\text{div}S_c$ does not show many points with high amplitude out of the fit line shows that ISM is not altered by high-frequency noise compared to TFM. Differently, BISM calculation is based on the integration of the surface force field \vec{f}_m . A perturbation in \vec{u} with wave vector \vec{q} results in a perturbation of the stress tensor ΔS_{tot} proportional to $1/q$. Low-frequency noise thus strongly alters the value of S_{tot} . And indeed, the regularization scheme in BISM calculation damps these low frequencies [Fig. 3(c)]. Thus, in this context, BISM is expected to be very sensitive to the boundary conditions.

D. Effect of boundaries conditions on BISM calculations

A proper choice of the boundary conditions also appeared to be critical for the success of BISM calculation. S_{tot} was either calculated when assuming zero stress at the edge of the thin plate or when fixing the boundary stress with the surface forces at the edge of the plate: $S_{\text{tot}} \cdot \vec{n} = \vec{f}_m$, with \vec{n} the normal to the edge of the plate. Only the appropriate boundary conditions brought the BISM curve close to the FEM curve [Fig. 3(d)].

V. BISM AND ISM ARE CONSISTENT WITH FEM

Stresses calculated with ISM and BISM approaches were compared to the FEM calculation. While S_c is a direct output of the FEM stress tensor calculation, S_{tot} was calculated as the difference between the resistive stress tensors of the adhered plate (S_c) and of the non adhered plate ($S_0 = -S_{\text{act}}$) as described in Sec. II. It was compared to BISM calculation whose value of the regularization parameter was chosen based on the noise level of \vec{f}_m (Fig. 3).

As shown in Fig. 2(c), S_{ISM} compared well with S_c in consistence with the thin plate assumption. Similarly, BISM did reconstruct S_{tot} by using appropriate boundary conditions and regularization parameter [Fig. 2(d)], both parameters having an important impact on the stress calculation as was detailed above.

VI. RELATIONSHIP BETWEEN $\text{DIV}S_c$ AND \vec{F}

In Ref. [9], we experimentally evidenced a linear relationship between $\text{div}(S_c)$ and \vec{f}_m , which entails another linear relationship between S_c and S_{tot} . We showed that these linear relationships could only be observed if the sizes of the adhesive active areas were smaller than the resolution of our analysis (i.e., 400 nm at best). Here our patches are necessarily above the resolution of our grid. But, we did try to run our modeling on a smaller Gaussian adhesive patch of $1 \mu\text{m}$ in size. Results are presented on Fig. 4. Again BISM and ISM are nicely recovered [Figs. 4(a) and 4(b)], but we do not recover the linear relationship between $\text{div}(S_c)$ and \vec{f}_m [Fig. 4(d)]. This is normal as the size of the patches are necessarily larger than the sampling size fixed by the mesh. However, when reducing these sizes, the relationship tends toward more linear (compare the blue and red lines).

VII. CASE OF LOCALIZED ADHESION

We then examined the case where the cells do not adhere everywhere. We tested how this situation would impact the correlation between $\text{div}S_{\text{ISM}}$ and \vec{f}_m . It should be noted that out of the areas where the cell is adhered, S_{ISM} differs from S_c as its calculation is based on the deformation of the substrate which now differs from the deformation of the cell. Using 3D FEM simulations, we observed that the surface forces \vec{f}_m concentrate in the regions of adhesion only [Fig. 5(a)]. Would intracellular stress generation occur out of the adhered areas, the surface forces \vec{f}_m would change in amplitude but of course they would still concentrate into the adhesive patches. As a result, it could not be inferred by the calculation of the total

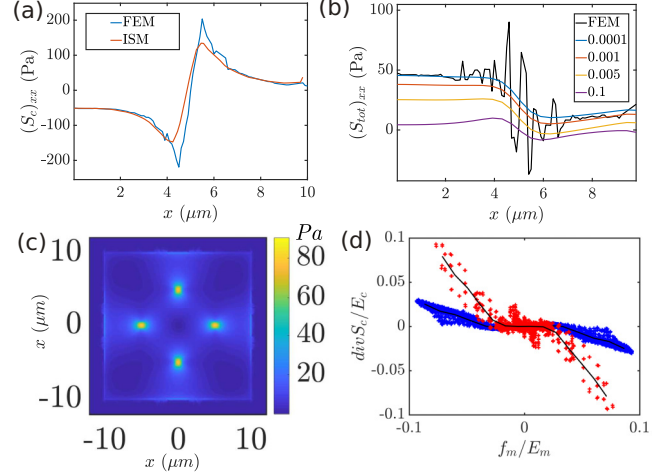


FIG. 4. Comparison of (a) S_{ISM} and (b) S_{BISM} with S_c and S_{tot} calculated with FEM simulations for a uniformly adhered plate subjected to a local force field \vec{f}_{act} of Gaussian distribution with similar design as in Fig. 2, but of smaller size (force patch of $1 \mu\text{m}$, $\sigma = 0.25 \mu\text{m}$). Again, ISM and BISM well account for the values of S_c (blue line) and S_{tot} (black line). Influence of the value of regularization parameter on the shape of S_{BISM} is shown in panel (b) (values are listed in the legend). (c) Surface forces \vec{f}_m . (d) Correlation of $\text{div}S_c$ and \vec{f}_m . The sampling size is imposed by the mesh size and is smaller than the width of the Gaussian field (blue: force patch of $5 \mu\text{m}$, $\sigma = 2 \mu\text{m}$; red: force patch of $1 \mu\text{m}$, $\sigma = 0.25 \mu\text{m}$). The black lines are bin averages of the blue or red points.

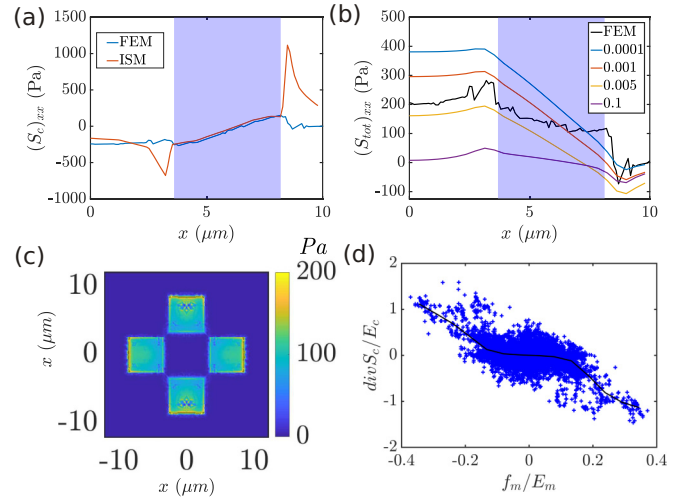


FIG. 5. Comparison of (a) S_{ISM} and (b) S_{BISM} with S_c and S_{tot} calculated with FEM simulations for a plate only adhered in the patches where active surface forces apply. The characteristics of the active force field is identical to Fig. 2 in the main text (force patch of $5 \mu\text{m}$, $\sigma = 2 \mu\text{m}$). Here ISM is no more relevant out of the adhered patch and BISM also fails to represent S_{tot} (shown with a black line). The adhesive area is delimited by the light purple area in both panels (a) and (b). Influence of the value of the regularization parameter on the shape of S_{BISM} is shown in panel (b) (values are listed in the legend). (c) Amplitude map of the surface forces \vec{f}_m for a plate that is only adhered through the local patches where the active forces \vec{f}_{act} are generated (force patch of $5 \mu\text{m}$, $\sigma = 2 \mu\text{m}$). (d) Correlation between $\text{div}S_c$ and \vec{f}_m for the locally adhered plate [same parameters as in panel (a)].

stress hS_{tot} as Eq. (4) does not contain any information on the location of the stress generators. Thus, as expected, the calculation of S_{tot} is less robust when the cell is not continuously adhered (Fig. 5). $\text{div}S_{\text{ISM}}$ and \vec{f}_m showed a correlation that resembles the one obtained for adherent cells in the presence of force generators of width larger than the sampling size, although it appeared more noisy [compare Figs. 4(d) and 5(d)]. Thus, the experimental observation of a linear relationship between $\text{div}S_{\text{ISM}}$ and \vec{f}_m may not be sufficient to conclude on the adhesive interaction of the cells with the substrate, the measure of transmitted surface forces \vec{f}_m that emerge from the noise being more conclusive. The intracellular stresses generated in regions where the level of force transmission to the substrate is low thus remain difficult to characterize by these mechanical approaches.

VIII. CONCLUSION

We proposed here a set of 3D FEM simulations to test and validate intracellular stress calculations that are done by two independent techniques, ISM and BISM, which address two different stresses. We showed that BISM enables to measure

the total stress inside the cells, while ISM retrieves the resistive component of the stress. We delineated the framework within which these techniques provide consistent information: for both techniques, the calculation infers relevant stresses only at the locations where the cells are adherent; concerning BISM, a proper quantification of the noise level to select the optimal regularization parameter and a proper definition of the boundary conditions are mandatory. Within this well-defined framework, we have shown that both approaches bring valuable and complementary information on intracellular stresses which then allow the retrieval of the active part of the intracellular stress. Taking advantage of this knowledge, it is now possible to analyze intracellular stresses in real experiments. This is what we have done in a companion paper [9].

ACKNOWLEDGMENTS

The authors are indebted to P. Marcq for the provision of the BISM calculation code. This work was initiated by very fruitful discussions with E. Mazza, L. Filotto, P. Silberzan, and T. Vourc'h. H.D.-A. and A.N. are grateful to them. A.N. acknowledges the support by Grant No. ANR-12-JSV5-0008.

-
- [1] P. Friedl and D. Gilmour, *Nat. Rev. Mol. Cell Biol.* **10**, 445 (2009).
 - [2] S. van Helvert, C. Storm, and P. Friedl, *Nat. Cell Biol.* **20**, 8 (2018).
 - [3] V. Hakim and P. Silberzan, *Rep. Prog. Phys.* **80**, 076601 (2017).
 - [4] U. S. Schwarz and S. A. Safran, *Rev. Mod. Phys.* **85**, 1327 (2013).
 - [5] C. E. Chan and D. J. Odde, *Science* **322**, 1687 (2008).
 - [6] M. Dembo and Y.-L. Wang, *Biophys. J.* **76**, 2307 (1999).
 - [7] U. S. Schwarz, N. Balaban, D. Riveline, A. Bershadsky, B. Geiger, and S. Safran, *Biophys. J.* **83**, 1380 (2002).
 - [8] J. Notbohm, S. Banerjee, K. J. Utuje, B. Gweon, H. Jang, Y. Park, J. Shin, J. P. Butler, J. J. Fredberg, and M. C. Marchetti, *Biophys. J.* **110**, 2729 (2016).
 - [9] H. Delanoë-Ayari, N. Bouchonville, M. Courçon, and A. Nicolas, *Phys. Rev. Lett.* **129**, 098101 (2022).
 - [10] N. Wang, I. M. Toli-Nørrelykke, J. Chen, S. M. Mijailovich, J. P. Butler, J. J. Fredberg, and D. Stamenović, *Amer. J. Physiol.-Cell Physiol.* **282**, C606 (2002).
 - [11] D. T. Tambe, C. Corey Hardin, T. E. Angelini, K. Rajendran, C. Y. Park, X. Serra-Picamal, E. H. Zhou, M. H. Zaman, J. P. Butler, D. A. Weitz, J. J. Fredberg, and X. Trepat, *Nat. Mater.* **10**, 469 (2011).
 - [12] V. Nier, S. Jain, C. T. Lim, S. Ishihara, B. Ladoux, and P. Marcq, *Biophys. J.* **110**, 1625 (2016).
 - [13] M. Moussus, C. der Loughian, D. Fuard, M. Courçon, D. Gulino-Debrac, H. Delanoë-Ayari, and A. Nicolas, *Soft Matter* **10**, 2414 (2014).
 - [14] U. S. Schwarz and J. R. Soiné, *Biochimica et Biophysica Acta* **1853**, 3095 (2015).
 - [15] S. Timoshenko and J. N. Goodier, *Theory of Elasticity*, 2nd ed. (McGraw-Hill, New York, 1951).
 - [16] D. T. Tambe, U. Croutelle, X. Trepat, C. Y. Park, J. H. Kim, E. Millet, J. P. Butler, and J. J. Fredberg, *PLoS ONE* **8**, e55172 (2013).
 - [17] L. D. Landau and E. M. Lifshitz, *Theory of Elasticity*, 2nd ed., Course of Theoretical Physics, Vol. 7 (Pergamon Press, Oxford, 1970).
 - [18] S. Tlili, M. Durande, C. Gay, B. Ladoux, F. Graner, and H. Delanoë-Ayari, *Phys. Rev. Lett.* **125**, 088102 (2020).
 - [19] M. Moussus, C. der Loughian, D. Fuard, M. Courçon, D. Gulino-Debrac, H. Delanoë-Ayari, and A. Nicolas, *Soft Matter* **10**, 7683 (2014).
 - [20] B. Sabass, M. L. Gardel, C. M. Waterman-Storer, and U. S. Schwarz, *Biophys. J.* **94**, 207 (2008).
 - [21] See https://github.com/heleneayari/Active_passive_stresses.
 - [22] J. P. Butler, I. Tolić-Nørrelykke, B. Fabry, and J. J. Fredberg, *Amer. J. Physiol.-Cell Physiol.* **282**, C595 (2002).
 - [23] A. Caboussat and R. Glowinski, *J. Comput. Math.* **30**, 354 (2021).
 - [24] D. Ambrosi, *SIAM J. Appl. Math.* **66**, 2049 (2006).